Publication Year	2010
Acceptance in OA	2023-01-23T11:56:52Z
Title	The Photodetector Array Camera and Spectrometer (PACS) on the Herschel Space Observatory
Authors	Poglitsch, A., Waelkens, C., Geis, N., Feuchtgruber, H., Vandenbussche, B., Rodriguez, L., Krause, O., Renotte, E., van Hoof, C., Saraceno, P., Cepa, J., Kerschbaum, F., Agnèse, P., Ali, B., Altieri, B., Andreani, P., Augueres, J. -L., Balog, Z., Barl, L., Bauer, O. H., Belbachir, N., BENEDETTINI, Milena, Billot, N., Boulade, O., Bischof, H., Blommaert, J., Callut, E., Cara, C., Cerulli, R., Cesarsky, D., Contursi, A., Creten, Y., De Meester, W., Doublier, V., Doumayrou, E., Duband, L., Exter, K., Genzel, R., Gillis, J. -M., Grözinger, U., Henning, T., Herreros, J., Huygen, R., Inguscio, M., Jakob, G., Jamar, C., Jean, C., de Jong, J., Katterloher, R., Kiss, C., Klaas, U., Lemke, D., Lutz, D., Madden, S., Marquet, B., Martignac, J., Mazy, A., Merken, P., Montfort, F., MORBIDELLI, LORENZO, Müller, T., Nielbock, M., Okumura, K., Orfei, R., Ottensamer, R., PEZZUTO, Stefano, Popesso, P., Putzeys, J., Regibo, S., Reveret, V., Royer, P., Sauvage, M., Schreiber, J., Stegmaier, J., Schmitt, D., Schubert, J., Sturm, E., Thiel, M., Tofani, G., Vavrek, R., Wetzstein, M., Wieprecht, E., Wiezorrek, E.
Publisher's version (DOI)	10.1051/0004-6361/201014535
Handle	http://hdl.handle.net/20.500.12386/32981
Journal	ASTRONOMY & ASTROPHYSICS
Volume	518

A&A 518, L2 (2010)
DOI: 10.1051/0004-6361/201014535

Astronomy & Astrophysics
Special feature

Herschel: the first science highlights

Letter to the Editor

The Photodetector Array Camera and Spectrometer (PACS) on the *Herschel* Space Observatory⋆

A. Poglitsch[1], C. Waelkens[2], N. Geis[1], H. Feuchtgruber[1], B. Vandenbussche[2], L. Rodriguez[3], O. Krause[4], E. Renotte[5], C. van Hoof[6], P. Saraceno[7], J. Cepa[8], F. Kerschbaum[9], P. Agnèse[17], B. Ali[19], B. Altieri[15], P. Andreani[12,16], J.-L. Augueres[3], Z. Balog[4], L. Barl[1], O. H. Bauer[1], N. Belbachir[10], M. Benedettini[7], N. Billot[3], O. Boulade[3], H. Bischof[11], J. Blommaert[2], E. Callut[5], C. Cara[3], R. Cerulli[7], D. Cesarsky[1], A. Contursi[1], Y. Creten[6], W. De Meester[2], V. Doublier[1], E. Doumayrou[3], L. Duband[18], K. Exter[2], R. Genzel[1], J.-M. Gillis[5], U. Grözinger[4], T. Henning[4], J. Herreros[8], R. Huygen[2], M. Inguscio[13], G. Jakob[1,12], C. Jamar[5], C. Jean[2], J. de Jong[1], R. Katterloher[1], C. Kiss[20], U. Klaas[4], D. Lemke[4], D. Lutz[1], S. Madden[3], B. Marquet[5], J. Martignac[3], A. Mazy[5], P. Merken[6], F. Montfort[5], L. Morbidelli[14], T. Müller[1], M. Nielbock[4], K. Okumura[3], R. Orfei[7], R. Ottensamer[9,11], S. Pezzuto[7], P. Popesso[1], J. Putzeys[6], S. Regibo[2], V. Reveret[3], P. Royer[2], M. Sauvage[3], J. Schreiber[4], J. Stegmaier[4], D. Schmitt[3], J. Schubert[1], E. Sturm[1], M. Thiel[1], G. Tofani[14], R. Vavrek[15], M. Wetzstein[1], E. Wieprecht[1], and E. Wiezorrek[1]

[1] Max-Planck-Institut für extraterrestrische Physik, Giessenbachstraße, 85748 Garching, Germany
e-mail: alpog@mpe.mpg.de
[2] Institute of Astronomy KU Leuven, Celestijnenlaan 200D, 3001 Leuven, Belgium
[3] Commissariat à l'Energie Atomique, IRFU, Orme des Merisiers, Bât. 709, 91191 Gif/Yvette, France
[4] Max-Planck-Institut für Astronomie, Königstuhl 17, 69117 Heidelberg, Germany
[5] Centre Spatial de Liège, Parc Scientifique du Sart Tilman, Avenue du Pré-Aily, 4031 Angleur-Liège, Belgium
[6] Interuniversity Microelectronics Center, Kapeldreef 75, 3001 Leuven, Belgium
[7] Istituto di Fisica dello Spazio Interplanetario, Via del Fosso del Cavaliere, 00133 Roma, Italy
[8] Instituto de Astrofisica de Canarias, C/via Lactea s/n, La Laguna, 38200 Santa Cruz de Tenerife, Spain
[9] Institut für Astronomie der Universität Wien, Türkenschanzstraße 17, 1180 Wien, Austria
[10] AIT Austrian Institute of Technology, Donau-City-Straße 1, 1220 Wien, Austria
[11] Institute of Computer Vision and Graphics, Graz University of Technology, Inffeldgasse 16/II, 8010 Graz, Austria
[12] European Southern Observatory, Karl-Schwarzschild-Str. 2, 85748 Garching, Germany
[13] LENS - European Laboratory for Non-Linear Spectroscopy, Via Nello Carrara 1, 50019 Sesto-Fiorentino (Firenze), Italy
[14] Osservatorio Astrofisico di Arcetri, Largo E. Fermi 5, 50125 Firenze, Italy
[15] European Space Astronomy Centre (ESAC), Camino bajo del Castillo, s/n, Villanueva de la Cañada, 28692 Madrid, Spain
[16] Osservatorio Astronomico di Trieste, via Tiepolo 11, 34143 Trieste, Italy
[17] Commissariat à l'Energie Atomique, LETI, 17 rue des Martyrs, 38054 Grenoble, France
[18] Commissariat à l'Energie Atomique, INAC/SBT, 17 rue des Martyrs, 38054 Grenoble, France
[19] NASA *Herschel* Science Center, Pasadena, USA
[20] Konkoly Observatory, PO Box 67, 1525 Budapest, Hungary

Received 29 March 2010 / Accepted 28 April 2010

ABSTRACT

The Photodetector Array Camera and Spectrometer (PACS) is one of the three science instruments on ESA's far infrared and submillimetre observatory. It employs two Ge:Ga photoconductor arrays (stressed and unstressed) with 16×25 pixels, each, and two filled silicon bolometer arrays with 16×32 and 32×64 pixels, respectively, to perform integral-field spectroscopy and imaging photometry in the 60–210 μm wavelength regime. In photometry mode, it simultaneously images two bands, 60–85 μm or 85–125 μm and 125–210 μm, over a field of view of $\sim 1.75' \times 3.5'$, with close to Nyquist beam sampling in each band. In spectroscopy mode, it images a field of $47'' \times 47''$, resolved into 5×5 pixels, with an instantaneous spectral coverage of $\sim$ 1500 km s^{-1} and a spectral resolution of $\sim$175 km s^{-1}. We summarise the design of the instrument, describe observing modes, calibration, and data analysis methods, and present our current assessment of the in-orbit performance of the instrument based on the performance verification tests. PACS is fully operational, and the achieved performance is close to or better than the pre-launch predictions.

Key words. space vehicles: instruments – instrumentation: photometers – instrumentation: spectrographs

1. Introduction

The PACS instrument was designed as a general-purpose science instrument covering the wavelength range ~60–210 μm. It

⋆ *Herschel* is an ESA space observatory with science instruments provided by European-led Principal Investigator consortia and with important participation from NASA.

features both, a photometric multi-colour imaging mode, and an imaging spectrometer. Both instrument sections were designed with the goal of maximising the science return of the mission, given the constraints of the *Herschel* platform (telescope at $T \approx 85$ K, diffraction limited for $\lambda > 80\,\mu$m, limited real estate on the cryostat optical bench) and available FIR detector technology.

1.1. Photometer rationale

Photometric colour diagnostics requires spectral bands with a relative bandwidth $\Delta\lambda/\lambda < 0.5$. In coordination with the longer wavelength SPIRE bands, the PACS photometric bands have been defined as 60−85 μm, 85−130 μm, and 130−210 μm, each spanning about half an octave in frequency.

A large fraction of the *Herschel* observing time will be spent on deep and/or large scale photometric surveys. For these, mapping efficiency is of the highest priority. Mapping efficiency is determined by both, the field of view of the instrument (in the diffraction-sampled case, the number of pixels) and the sensitivity per pixel. The PACS photometer was therefore designed around the largest detector arrays available without compromising sensitivity.

Simultaneous observation of several bands immediately multiplies observing efficiency. By implementing two camera arrays, PACS can observe a field in two bands at a time.

Extracting very faint sources from the bright telescope background requires means to precisely flat-field the system responsivity on intermediate time-scales, as well as the use of spatial modulation techniques (chopping/nodding, scan-mapping) to move the signal frequency from "DC" into a domain above the $1/f$ "knee" of the system, including – most notably – the detectors.

1.2. Spectrometer rationale

Key spectroscopic observations, particularly of extragalactic sources, ask for the detection of faint spectral lines with medium resolution ($R \sim 1500$).

The power emitted or absorbed by a single spectral line in the far-infrared is normally several orders of magnitudes lower than the power in the dust continuum over a typical photometric band. Sensitivity is thus the most important parameter for optimisation; with background-limited detector performance the best sensitivity is obtained if the spectrometer satisfies the following conditions: the detection bandwidth should not be greater than the resolution bandwidth, which in turn should be matched to the line width of the source, and, the line flux from the source must be detected with the highest possible efficiency in terms of system transmission, spatial and spectral multiplexing.

Again, subtraction of the high telescope background has to be achieved by appropriate spatial and/or spectral modulation techniques.

2. Instrument design

The instrument is divided into optically well separated compartments: a *front optics section*, common to all optical paths through the instrument, containing grey-body calibration sources and a chopper, each at an intermediate image of the telescope secondary. Thereafter follow the separate *photometer camera* and *spectrometer* sections. The whole instrument (Fig. 1) – except the detectors – is kept at the "Level 1" temperature of ~3 to 5 K provided by the satellite.

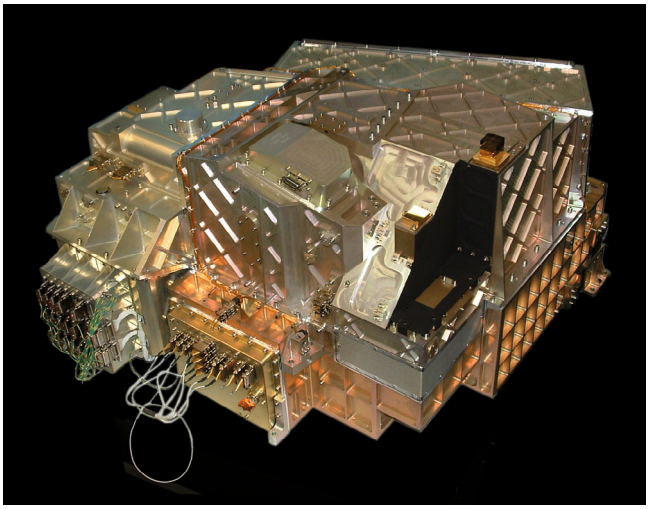

Fig. 1. The PACS focal plane unit (Qualification Model).

2.1. Front optics

The front optics (see Fig. 2) has several instrument wide tasks: it provides for an intermediate image of the telescope secondary mirror (the entrance pupil of the telescope) with the cold Lyot stop and the first blocking filter, common to all instrument channels. A further image of the pupil is reserved for the focal plane chopper; this allows spatial chopping with as little as possible modulation in the background received by the instrument, and it allows the chopper – through two field mirrors adjacent to the field stop in the telescope focal plane – to switch between a (chopped) field of view on the sky and two calibration sources (see also Fig. 3).

In an intermediate focus after the chopper, a fixed field mirror splits off the light for the spectroscopy channel. The remaining part of the field of view passes into the photometry channels. A "footprint" of the focal-plane splitter is shown in Fig. 4.

The calibrators are placed near the entrance to the instrument, outside of the Lyot stop, to have approximately the same light path for observation and internal calibration. The calibrator sources are grey-body sources providing FIR radiation loads slightly above or below the telescope background, respectively. They uniformly illuminate both, the field of view, and the Lyot stop, to mimic the illumination by the telescope.

The chopper provides a maximum throw of 6′ on the sky; this allows full separation of an "object" field from a "reference" field. The chopper (Krause et al. 2006) is capable of following arbitrary waveforms with a resolution of 1″ and delivers a duty-cycle of ~80% at a chop frequency of 5 Hz.

2.2. Imaging photometer

After the intermediate focus provided by the front optics, the light is split into the long-wave ("red") and short-wave ("blue", "green") channels by a dichroic beam-splitter with a transition wavelength of 130 μm (design value) and is re-imaged with different magnification onto the respective bolometer arrays.

The 32×16 (red) or 64×32 (blue/green) pixels in each array are used to image the same field of view of $3.5' \times 1.75'$, the different magnification providing full beam sampling at 90 μm and 180 μm, respectively. Projected onto the sky, pixel sizes are $6.4'' \times 6.4''$ (red) and $3.2'' \times 3.2''$ (blue/green), respectively. The red band (130−210 μm) can be combined with either the blue or the green channel, 60−85 μm or 85−130 μm, for simultaneous

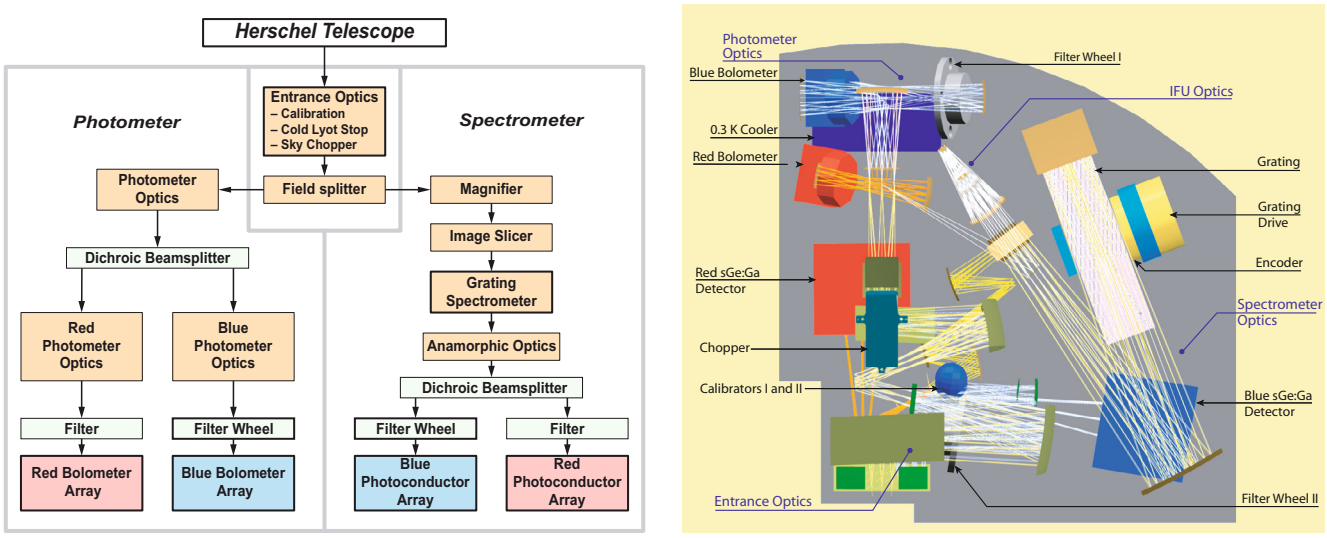

Fig. 2. *Left: PACS focal plane unit (FPU) functional block diagram.* The arrows visualise the optical paths through the instrument. Imaging optics and filter components are shown in different colours; active components (mechanisms, electronics) are outlined in bold. *Right: PACS FPU layout.* After the common entrance optics with calibrators and the chopper, the field is split into the spectrometer train and the photometer trains. The two *bolometer cameras* (*top*) have partially separate re-imaging optics split by a dichroic beam splitter; the short wavelength camera band is further split up by two filters on filter wheel I. In the *spectrometer train*, the integral field unit (image slicer, *middle*) first converts the square field into an effective long slit for the Littrow-mounted grating spectrograph (*on the right*). The dispersed light is distributed to the two photoconductor arrays by a dichroic beam splitter between the 1st and 2nd orders, then the 2nd or 3rdorder for the short-wave array is chosen by filter wheel II.

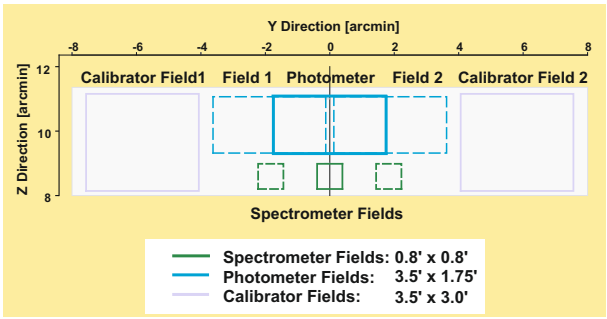

Fig. 3. *PACS telescope focal plane usage.* Long- and short-wavelength photometry bands are coincident. The smaller spectrometer field of view is offset in the -*Z* direction. Chopping is along the *Y* axis (*left-right*). On both sides of the sky area in the focal plane the internal calibrators are reachable by the chopper. The maximum chopper amplitude for sky observations (used in spectroscopy) is ±3′.

observation. Blue and green are selected by filter wheel. All filters in PACS are implemented as multi-mesh filters and provided by Cardiff University[1] (Ade et al. 2006).

2.2.1. Bolometer arrays

The PACS bolometers are filled arrays of square pixels which allow instantaneous beam sampling. 4×2 monolithic sub-arrays of 16×16 pixels each are tiled together to form the blue/green focal plane array (see Fig. 4). There remains a small gap between sub-arrays, which has to be filled by mapping methods (rastering, scanning). Similarly, two sub-arrays of 16 × 16 pixels are form the red focal plane array. The bolometer assemblies are kept at "Level 0" cryostat temperature (~1.65 K).

The bolometer sub-arrays themselves are mounted thermally isolated from the surrounding 2 K structure and at an operating temperature of 0.3 K. This is provided by the closed cycle ^{3}He sorption cooler (Duband et al. 2008), designed to support uninterrupted operation of the bolometers for two days. After this period, a recycling is required. This process is usually carried out during the daily telecommunication period of the satellite. Bolometer cameras and cryo-cooler are mounted together in a self contained subunit of the FPU.

The cold readout electronics of the bolometers is split in two levels; a first stage is on the back of the focal plane arrays, operating at 0.3 K, and a second buffer stage runs at 2 K. The multiplexing readout samples each pixel at a rate of 40 Hz.

The post-detection bandwidth (thermal/electrical) of the bolometers is ~5 Hz at nominal bias and can be traded off against NEP; the noise of the bolometer/readout system, however, has a strong $1/f$ component. To achieve optimum sensitivity, observations have to be executed such that the signal modulation due to chopping or scanning falls primarily in the frequency band from 1 Hz to 5 Hz, where close to background-limited performance is achieved. Details on the bolometer design have been published in Agnese et al. (1999, 2003); Simoens et al. (2004); Billot et al. (2007).

2.3. Integral field spectrometer

In the spectrometer, we use an integral field unit (IFU) feeding a Littrow-mount grating spectrometer to collect an instantaneous 16-pixel spectrum with reasonable sampling and baseline coverage for each of the 5 × 5 spatial image pixels.

The IFU concept has been selected because simultaneous spectral and spatial multiplexing allows for the most efficient detection of weak individual spectral lines with sufficient baseline coverage and high tolerance to pointing errors without compromising spatial resolution, as well as for spectral line mapping of extended sources regardless of their intrinsic velocity structure.

It is possible to operate both spectrometer detector arrays simultaneously. For wide scans, full spectra can so be obtained in both selected grating orders. In a spectral line mode in the

[1] P.A.R. Ade, Department of Physics and Astronomy, University of Wales, Cardiff, UK.

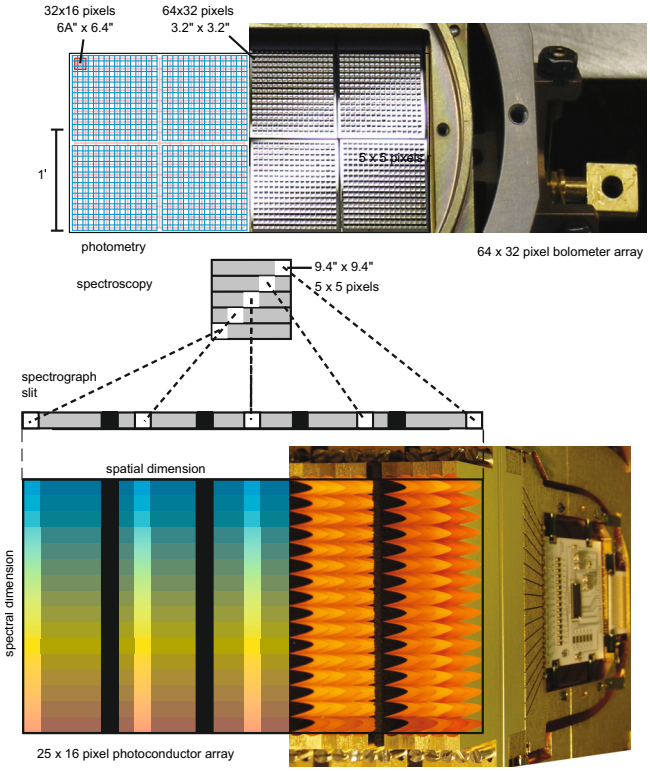

Fig. 4. *Field splitter footprint and detectors*. A fixed mirror splits the focal plane into the photometry (*top*) and spectroscopy (*bottom*) channels of the instrument. The two photometer cameras have different magnification to cover the same field of view with a different pixel scale. In spectroscopy, an optical image slicer re-arranges the 2-dimensional field along the entrance slit of the grating spectrograph such that for each spatial element in the field of view, a spectrum can be simultaneously observed with a 2D detector array. *Right*: the close-up photos show, at the appropriate scale, half of the blue/green bolometer array with its tiled monolithic sub-arrays (see 2.2.1) and part of the red photoconductor array with its area-filling light-cones and CREs (see 2.3.1).

grating order-of-interest, the other array yields narrow-band continuum data, or in suitably line-rich sources, serendipitous lines.

The spectrometer covers the wavelength range 55−210 μm, with simultaneous imaging of a 47″ × 47″ field of view in two grating orders, resolved into 5 × 5 pixels. The spectral resolving power of 1000−4000 (Δv = 75−300 km s^{-1}) with an instantaneous coverage of ∼1500 km s^{-1}, depends on wavelength and order. A detailed resolution curve is given in the PACS observers' manual (2010).

In the IFU, an image slicer employing reflective optics is used to re-arrange the 2-dimensional field of view along a 1×25 pixels entrance slit for a grating spectrometer, as schematically shown in Fig. 4. A detailed description of the slicer optics, including a physical optics analysis, is given in a paper on the similar SOFIA experiment FIFI LS (Looney et al. 2003).

The Littrow-mounted grating with a length of ∼300 mm is operated in 1st, 2nd or 3rd order, respectively, to cover the full wavelength range. Nominally, the 1st order covers the range 105−210 μm, the 2nd order 72−105 μm, and the 3rd order 55−72 μm (design values – actual filter edges slightly deviate from these). Anamorphic collimating optics expands the beam along the grating over a length required to reach the desired spectral resolution. The grating is actuated by a cryogenic motor (Renotte et al. 1999) which, together with arc-second precision position readout and control, allows spectral scanning/stepping for improved spectral flat-fielding and for coverage of extended wavelength ranges. The settling time for small motions is ≤32 ms, enabling wavelength-switching observations.

Anamorphic re-imaging optics after the grating spectrometer allows one to independently match the dispersed image of the slit spatially to the 25 pixel columns and adjust the dispersion such that the square pixels of the detector arrays well sample the spectral resolution.

The light from the 1st diffraction order is separated from the higher orders by a dichroic beam splitter and passed on into two optical trains feeding the respective detector array (stressed/unstressed) for the wavelength ranges 105−210 μm and 55−105 μm. The filter wheel in the short-wavelength path selects 2nd or 3rd grating order.

2.3.1. Photoconductor arrays

The 25×16 pixels Ge:Ga photoconductor arrays employed in the spectrometer are a completely modular design. 25 linear modules of 16 pixels each are stacked together to form a contiguous, 2-dimensional array. Each of the modules records an instantaneous spectrum of 16 pixels, as described above.

Light cones in front of the actual detector block provide area-filling light collection in the focal plane. Details of the design of both arrays are given in Kraft et al. (2000, 2001); Poglitsch et al. (2003).

Responsivity measurements of both stressed and unstressed modules show sufficiently homogeneous spectral and photometric response within each module and between modules. Absolute responsivity calibration for optimum bias under in-orbit conditions is under way and will most likely give numbers of ∼10 A/W for the unstressed detectors and ∼40 A/W for the stressed detectors. The detectors are operated at (stressed) or slightly above (unstressed) the "Level 0" cryostat temperature (∼1.65 K).

Each linear module of 16 detectors is read out by a cryogenic amplifier /multiplexer circuit (CRE) in CMOS technology (Merken et al. 2004). The readout electronics is integrated into the detector modules (see Fig. 4), but operates at "Level 1" temperature (3...5 K).

Measurements of the NEP of both arrays after integration into the instrument flight model at characteristic wavelengths and with representative flux levels have confirmed the performance measured at module level. Only a small fraction of pixels suffers from excess noise. Median NEP values are 8.9×10^{-18} W/Hz$^{1/2}$ for the stressed and 2.1×10^{-17} W/Hz$^{1/2}$ for the unstressed detectors, respectively.

The achievable in-orbit performance was expected to depend critically on the effects of cosmic rays on the detector response. Proton irradiation tests performed at the synchrotron source of the Université Catholique de Louvain (Louvain la Neuve, Belgium) complemented by a γ-radiation test programme at MPIA indicated that NEPs close to those measured without irradiation should actually be achievable in flight (Katterloher et al. 2006; Stegmaier et al. 2008).

2.4. Instrument control electronics and on-board data processing

The warm electronics units of PACS on the satellite bus have several tasks: control the instrument, send the housekeeping and science data, and provide autonomy in the 20 hour interval between the daily telemetry periods. PACS is far too complex to

be controlled by a single electronics unit. Therefore, the various functions have been grouped into different subunits.

The Digital Processing Unit (DPU) provides the interface of PACS to the satellite and is therefore responsible for receiving and decoding commands from the ground or the mission timeline on-board. Decoded commands are forwarded by the DPU to the appropriate subsystems for execution. The DPU monitors the correct execution of all commands and raises errors should a failure occur. In the opposite data flow direction, all housekeeping and science data from the various subsystems of PACS are collected by the DPU, formatted into telemetry packets and sent to the satellite mass memory.

The DEtector and MEchanism Controller (DECMEC) receives and handles all low level commands to all PACS systems, except for the bolometers. Also, tasks that need to be synchronous (e.g., detector readouts, chopper motion, grating steps) are triggered from here. The DEC part operates the photoconductor arrays and receives their raw data, which arrive at 256 Hz for each pixel. It also receives the digitised bolometer data from BOLC (see below). The data are then sent on to the SPU (see below) for processing. The MEC part contains drivers for all mechanisms and regulated temperatures in the FPU and generates most of the instrument housekeeping data.

The BOLometer Controller (BOLC) operates the bolometer arrays and provides a clock signal to MEC for the chopper synchronisation in photometer mode. The digitised bolometer signals are sent to the SPU via DECMEC for processing.

The Signal Processing Unit (SPU) reduces the raw data rate from the detector arrays, which exceeds the average allowed telemetry rate of 130 kb/s by far. The SPU performs real-time reduction of the raw data in the time domain, bit rounding, and subsequent lossless compression. The algorithms employed (Ottensamer & Kerschbaum 2008) are optimised for each type of detector and observing mode to keep as true to the original raw data as possible.

3. Observing modes

Typical PACS observation days (OD) contain predominantly either photometer or spectrometer observations to optimise the observing efficiency within a photometer cooler cycle (see Sect. 5). After each cooler recycling procedure (which takes about 2.5 h), there are about 2.5 ODs of PACS photometer – prime or parallel mode – observations possible. Mixed days with both sub-instruments, e.g., to observe the same target in photometry and spectroscopy close in time, are only scheduled in exceptional cases.

3.1. Photometer

Three observing modes or astronomical observing templates (AOT) are validated on the PACS photometer side: (i) point-source photometry mode in chopping-nodding technique; (ii) scan map technique (for point-sources, small and large fields); (iii) scan map technique within the PACS/SPIRE parallel mode. The originally foreseen "small source mode" and "large raster mode" in chopping-nodding technique are replaced by the scan-map technique for better performance and sensitivity reasons.

All photometer configurations perform dual-band photometry with the possibility to select either the blue (60−85 μm) or the green (85−125 μm) filter for the short wavelength band, the red band (125−210 μm) is always included. The two bolometer arrays provide full spatial sampling in each band.

During an observation the bolometers are read-out with 40 Hz, but due to satellite data-rate limitations there are on-board reduction and compression steps needed before the data is down-linked. In PACS prime modes the SPU averages 4 subsequent frames; in case of chopping the averaging process is synchronised with the chopper movements to avoid averaging over chopper transitions. In PACS/SPIRE parallel mode 8 consecutive frames are averaged in the blue/green bands and 4 in the red band. In addition to the averaging process there is a supplementary compression stage "bit rounding" for high gain observations required, where the last n bits of the signal values are rounded off. The default value for n is 2 (quantisation step of 2×10^{-5} V or 4 ADU) for all high gain PACS/SPIRE parallel mode observations, 1 for all high gain PACS prime mode observations, and 0 for all low gain observations.

The selection of the correct gain ("LOW" or "HIGH") is driven by source flux estimates given by the observer. The switch to low gain is required for the flux limits given in Table 4. Each observation – chop-nod or scan-map – can be repeated several times, driven by the observer-specified repetition factor.

Each PACS photometer observation is preceded by a 30 s chopped calibration measurement executed during the target acquisition phase[2]. The chopper moves with a frequency of 0.625 Hz between the two PACS internal calibration sources. 19 chopper cycles are executed, each chopper plateau lasts for 0.8 s (32 readouts on-board) producing 8 frames in the down-link. There are always 5 s idle-time between the calibration block and the on-sky part for stabilisation reasons.

3.1.1. Chop-nod technique

The PACS photometer chop-nod point-source mode uses the PACS chopper to move the source by about 50″, corresponding to the size of about 1 blue/green bolometer matrix or the size of about half a red matrix, with a chopper frequency of 1.25 Hz. The nodding is performed by a satellite movement of the same amplitude but perpendicular to the chopping direction.

On each nod-position the chopper executes 3 × 25 chopper cycles. The 3 sets of chopper patterns are either on the same array positions (no dithering) or on 3 different array positions (dither option). In the dither-option the chopper pattern is displaced in $\pm Y$-direction (along the chopper direction) by about 8.5″ (2 2/3 blue pixels or 1 1/3 red pixels). Each chopper plateau lasts for 0.4 s (16 readouts on-board) producing 4 frames per plateau in the down-link. The full 3 × 25 chopper cycles per nod-position are completed in less than 1 min. The pattern is repeated on the second nod-position. In case of repetition factors larger than 1, the nod-cycles are repeated in the following way (example for 4 repetitions): nodA-nodB-nodB-nodA-nodA-nodB-nodB-nodA to minimise satellite slew times.

The achieved sensitivities (see Table 5) are worse by a factor 1.5−2 compared to the preflight prediction, due to different operating parameters.

Despite the degraded sensitivity this mode has advantages for intermediately bright sources in the range 50 mJy to about 50 Jy: a small relative pointing error (RPE) of 0.3″ and high photometric reliability.

[2] Note: in early mission phases (until OD 150) long photometer observations were interleaved with additional calibration blocks.

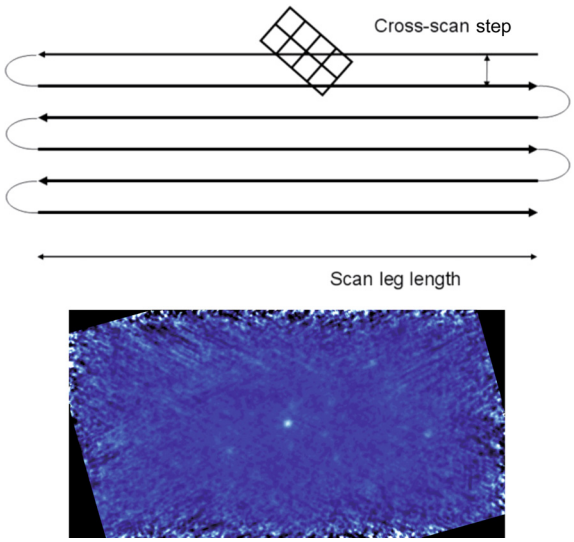

Fig. 5. *Top*: example of PACS photometer scan map. Schematic of a scan map with 6 scan line legs. After the first line, the satellite turns left and continue with the next scan line in the opposite direction. The reference scan direction is the direction of the first leg. *Bottom*: combined cross-scan mini-maps for HD 159330 (~30 mJy at 100 μm).

3.1.2. Scan technique

The scan-technique is the most frequently used *Herschel* observing mode. Scan maps are the default to map large areas of the sky, for galactic as well as extragalactic surveys, but meanwhile they are also recommended for small fields and even for point-sources. Scan maps are performed by slewing the spacecraft at a constant speed along parallel lines (see Fig. 5). Available satellite speeds are 10, 20, 60″/s in PACS prime mode and 20, 60″/s (slow, fast) in PACS/SPIRE parallel mode. The number of satellite scans, the scan leg length, the scan leg separation, and the orientation angles (in array and sky reference frames) are freely selectable by the observer. Via a repetition parameter the specified map can be repeated n times. The performance for a given map configuration and repetition factor can be evaluated beforehand via sensitivity estimates and coverage maps in HSPOT[3]. The PACS/SPIRE parallel mode sky coverage maps are driven by the fixed 21′ separation between the PACS and SPIRE footprints. This mode is very inefficient for small fields, the shortest possible observation requires about 45 min observing time.

During the full scan-map duration the bolometers are constantly read-out with 40 Hz, allowing for a complete time-line analysis for each pixel in the data-reduction on ground. A combination of two different scan directions is recommended for a better field and PSF reconstruction.

Most of the PACS prime observations are performed with a 20″/s scan speed where the bolometer performance is best and the pre-flight sensitivity estimates are met. For larger fields observed in instrument reference frame there is an option to use "homogeneous coverage" which computes the cross-scan distance in order to distribute homogeneously the time spent on each sky pixel in the map.

For short scan legs below about 10′ the efficiency of this mode drops below 50% due to the relatively long time required for the satellite turn-around (deceleration, idle-time, acceleration) between individual scan legs, which takes about 20 s for small leg separations of a few arcseconds. Nevertheless, this mode has an excellent performance for very small fields and even for point-sources (see Sect. 5 and Table 5).

The advantages of the scan mode for small fields are the better characterisation of the source vicinity and larger scale structures in the background, the more homogeneous coverage inside the final map, the higher redundancy with respect to the impact of noisy and dead pixels and the better point-source sensitivity as compared to a chop-nod observation of similar length.

[3] The *Herschel* observation planning tool is available from http://herschel.esac.esa.int/.

Table 1. Spectrometer calibration block key wavelengths.

Bands	Blue wavelength	Red wavelength
B2A / R1	60	120
B3A / R1	60	180
B2B / R1	75	150

Notes. The wavelengths observed in the spectrometer calibration block depend on the spectral bands visited in the rest of the observation.

3.2. Spectrometer

There are three validated PACS spectrometer observing modes: *chopped line spectroscopy* for single lines on sources with a clean background within 6′, *chopped range spectroscopy* for spectra over larger wavelength ranges on sources with a clean background within 6′, and the *wavelength switching mode*, for single lines on extended sources without clean background for chopping. An *unchopped observing mode* for larger wavelength ranges on extended sources is planned.

The three observing modes can be used in a single pointing, or repeated in a raster pattern on the sky. There are two sets of recommended raster patterns for mapping with full beam sampling: one for compact sources, which fit within the instantaneous FOV of the spectrometer, and one for more extended sources. For compact sources, the recommended pattern is a 3×3 raster with a 3″ step size in the blue bands and a 2×2 raster with a 4.5″ step size in the red band. For extended sources, $m \times n$ rasters with approximately 5/3 pixel step sizes in the blue bands and approximately 5/2 pixel step sizes in the red bands are recommended (see also PACS observers' manual 2010)

All spectrometer observing modes include a calibration block, a modulated measurement of the two internal calibration sources with the grating in a fixed position. The two sources are heated to different temperatures, hence provide different signal levels. The grating position is chosen to measure a reference wavelength in the bands that are measured in the sky observation. Table 1 lists these calibration block wavelengths.

The calibration block measurement starts during the slew of the spacecraft to the target in order to optimise the use of observing time.

Based on the continuum and line flux estimates entered by the observer, the expected maximum photoconductor signal level is estimated by the observing logic. For range spectroscopy, the expected flux at the maximum response is extrapolated via a Rayleigh-Jeans law from the reference wavelength and corresponding flux estimate. The appropriate integrating capacitance of the CRE is then chosen for the entire observation to avoid saturation.

Table 2. The wavelength range seen in a nominal line scan.

Band	λ	Full range		Every pixel	*FWHM*	
	(μm)	(km s^{-1})	(μm)	(μm)	(μm)	(km s^{-1})
B3A	55	1880	0.345	0.095	0.021	115
B3A	72	800	0.192	0.053	0.013	55
B2B	72	2660	0.638	0.221	0.039	165
B2B	105	1040	0.364	0.126	0.028	80
R1	105	5210	1.825	0.875	0.111	315
R1	158	2870	1.511	0.724	0.126	240
R1	175	2340	1.363	0.654	0.124	210
R1	210	1310	0.92	0.441	0.098	140

Notes. This range varies over the spectral bands. The column "every pixel" refers to the range that is seen by every spectral pixel.

3.2.1. Chopped line scan spectroscopy

The chopped line spectroscopy mode can contain up to 10 spectral line scans across different bands with the same fixed order selection filter wheel position. The diffraction grating is rotated over 43 to 48 steps so that every spectral pixel homogeneously samples one resolution element at least 3 times. This scan is repeated in two directions. This up/down scan can be repeated up to 10 times for a single line. Table 2 shows the wavelength range covered in the different bands.

At every grating position, the detector signal is modulated between on and off source via an on-off-off-on-on-off-off-on chopping pattern. At every chopper plateau two 1/8 second integrations of the photoconductor signals are recorded. The observer can choose a chopper throw of 6′, 3′ or 1′.

The sequence of line scans is repeated at two nod positions of the telescope. In the second nod position, the source is located on the off chopping position of the first nod in order to be able to determine the difference in telescope background at the two chop positions. The nod sequence can be repeated within one observation to increase the depth of the observation.

The line spectroscopy AOT provides a bright line mode. The sampling step size is identical to the nominal, faint line mode, but the number of steps in the scan is limited to 16. Therefore, in the bright line mode the range scanned is 1/3 of the ranges listed in Table 2.

3.2.2. Chopped range scan and SED spectroscopy

The chopped range scan AOT allows one to observe one or several spectral ranges. The mode provides two spectral sampling depth. The deep sampling uses the same sampling step size as the line spectroscopy mode and is typically used to measure broadened lines or ranges with several lines. The coarser Nyquist sampling depth provides a sampling of at least one sample in every half resolution element by one of the spectral pixels. Chopping frequency and scheme as well as the structure of the observation are the same as in line spectroscopy: a sequence of range scans is repeated in two nod positions, switching the source position between the two chopper positions.

Pre-defined ranges are foreseen to measure full PACS SEDs. These are measured in Nyquist sampling depth.

Repetitions of the same range within the nod position in Nyquist sampling depth are offset in wavelength, so that the same wavelength is sampled by different spectral pixels in every repetition.

3.2.3. Wavelength switching spectroscopy

The wavelength switching technique/mode is an alternative to the chopping/nodding mode, if by chopping to a maximum of 6′, the OFF position field-of-view cannot be on an emission free area, for instance in crowded areas.

In wavelength switching mode, the line is scanned with the same grating step as in chopped line spectroscopy, i.e., every spectral pixel samples at least every 1/3 of a resolution element. In wavelength switching we refer to this step as a dither step. At every dither step, the signal is modulated by moving the line over about half of the *FWHM*. This allows one to measure a differential line profile, canceling out the background. The modulation on every scan step follows an AABBBBAA pattern, where A is a detector integration at the initial wavelength, and B is a detector integration at the wavelength switching wavelength. This cycle is repeated 20 times in one direction, and repeated in the reverse wavelength direction. The switching amplitude is fixed for every spectral band.

In order to reconstruct the full power spectrum, a clean off-position is visited at the beginning and the end of the observation. On this position the same scan is performed. In between, the scan is performed at two or more raster positions.

4. Calibration

Prior to launch, the instrument has been exposed to an extensive ground based test and calibration programme. The resulting instrument characterisation has been determined in a specific test cryostat providing all necessary thermal and mechanical interfaces to the instrument. In addition to the PACS FPU, the cryostat hosted a telescope simulation optics, cryogenic far-infrared black-body sources, and a set of flip and chop mirrors. External to the test cryostat a methanol laser setup (Inguscio et al. 1986), movable hole masks with various diameters, illuminated by an external hot black-body and a water vapour absorption cell, have been available for measurements through cryostat windows. The results of this instrument level test campaign are summarised in Poglitsch et al. (2008) and served as a basis for the in-flight calibration in the performance verification phase of satellite and instruments.

4.1. Photometer

The absolute flux calibration of the photometer is based on models of fiducial stars (α Cet, α Tau, α CMa, α Boo, γ Dra, β Peg; Dehaes et al. 2010) and thermophysical models for a set of more than 10 asteroids (Müller & Lagerros 1998, 2002), building up on similar approaches for ISOPHOT (Schulz et al. 2002) and Akari-FIS (Shirahata et al. 2009). Together they cover a flux range from below 100 mJy up to 300 Jy. Both types of sources agree very well in all 3 PACS bands, and the established absolute flux calibration is consistent within 5%. The quoted photometric accuracies in Table 5 can thus be considered conservative. Neptune and Uranus with flux levels of several hundred Jansky are already close to the saturation limits, but have been used for flux validation purposes. At those flux levels, a reduction in response of up to 10% has been observed. For comparison, the latest FIR flux model of Neptune is considered to be accurate to better than 5% (Fletcher et al. 2010). No indications of any near- or mid-infrared filter leakage could be identified. Required colour corrections for the photometric PACS reference wavelengths (70, 100, 160 μm) which have been determined from the photometer filter transmission curves and bolometer responses

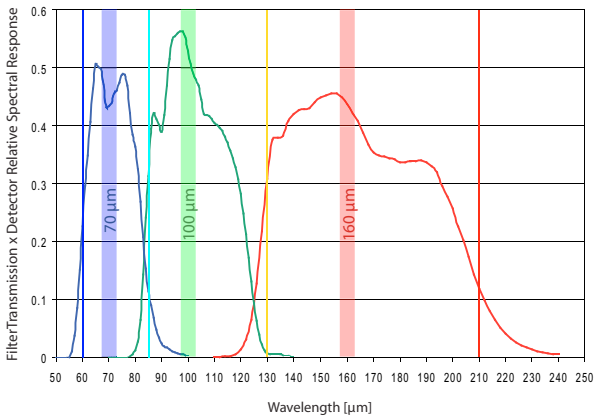

Fig. 6. Effective spectral response of the filter/detector chain of the PACS photometer in its three bands.

Table 3. Photometric colour corrections.

BB temp.	CC_70	CC_100	CC_160
BB (10 000 K)	1.02	1.03	1.07
BB (5000 K)	1.02	1.03	1.07
BB (1000 K)	1.01	1.03	1.07
BB (500 K)	1.01	1.03	1.07
BB (250 K)	1.01	1.02	1.06
BB (100 K)	0.99	1.01	1.04
BB (50 K)	0.98	0.99	1.01
BB (20 K)[a]	1.22	1.04	0.96
BB (15 K)	1.61	1.16	0.99
BB (10 K)	3.65	1.71	1.18
Power law (ν^{β})	CC_70	CC_100	CC_160
$\beta = -3.0$	1.04	1.04	1.06
$\beta = -2.0$	1.02	1.01	1.02
$\beta = -1.0$	1.00	1.00	1.00
$\beta = 0.0$	1.00	1.00	1.00
$\beta = 1.0$	1.00	1.01	1.03
$\beta = 2.0$	1.02	1.03	1.08
$\beta = 3.0$	1.04	1.07	1.14

Notes. [(a)] Colour corrections for sources with temperatures below 20 K can become quite significant, in particular at 70 μm.
Photometric reference spectrum: $\nu F_\nu = \lambda F_\lambda$ = const.. PACS bolometer reference wavelengths: 70.0, 100.0, 160.0 μm. In order to obtain a monochromatic flux density one has to divide the measured and calibrated band flux by the above tabulated values.

(see Fig. 6) are quite small. Suitable correction factors for a wide sample of SED shapes can be read from Table 3 but are also available from within the *Herschel* interactive processing environment. Absolute flux calibration uncertainties should improve over the mission, with better statistics of available celestial calibration observations.

The photometer focal plane geometry, initially established on ground by scanning a back-illuminated hole mask across the bolometer arrays, has been adapted to the actual telescope by optical modeling. The in-flight verification required a small change in scale and a slight rotation to fit to the results of a 32×32 raster on α Her. In particular these measurements also show that the possibilities to further improve the calibration of detailed distortions are limited by short-term pointing drifts of the satellite. Residual measured inter-band offsets between blue/green (0.3″) and green/red (1.2″) have been characterised and are implemented in the astrometric processing chain. Current best point spread functions (PSF) have been determined on asteroid Vesta.

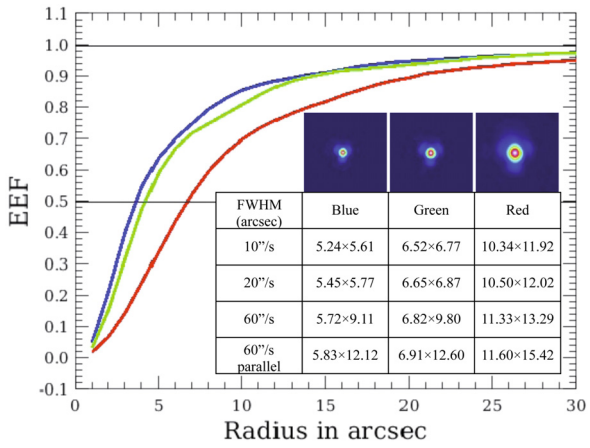

Fig. 7. Photometer encircled energy function for blue, green and red photometer bands, for 10″/s scan speed. The inset tabulates observed beam sizes (*FWHM*) as a function of scan speed. The bolometer time constant leads to an elongation in scan direction. Note that this elongation is additionally increased in SPIRE/PACS parallel observations, due to data compression (see also Sect. 5.1). The beam maps, shown for illustration, were taken at a 10″/s scan speed.

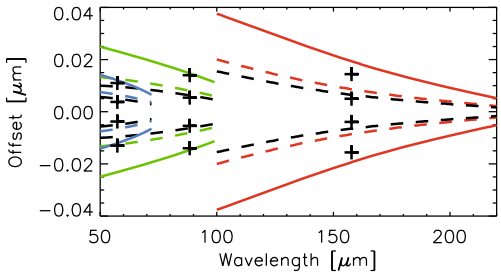

Fig. 8. Calculated wavelength offsets for point source positions: at the slit border (solid colour lines), for typical pointing errors up to 2″ (dashed colour lines) and measured line centre offsets for ±1.5″ (dashed black line and crosses) and slit border (black crosses) for three spectral lines on the point like planetary nebula IC 2501.

The observed 3-lobe structure of the PSF (Fig. 7 and Pilbratt et al. 2010) can be explained qualitatively by the secondary mirror support structure and has been verified in detail by ray tracing calculations taking the telescope design and known wave-front errors into account. The spatial resolution, expressed as encircled energy as a function of angular separation from PSF centre (Fig. 7), is in reasonable agreement with expectations from telescope and instrument design.

4.2. Spectrometer

The wavelength calibration of the PACS spectrometer relates the grating angle to the central wavelength "seen" by each pixel. Due to the finite width of the spectrometer slit, a characterisation of the wavelength scale as a function of (point) source position within the slit is required as well.

The calibration derived from the laboratory water vapour absorption cell is still valid in-flight. For ideal extended sources the required accuracy of better than 20% of a spectral resolution is met throughout all bands. While at band borders, due to leakage effects and lower S/N, the rms calibration accuracy is closer to 20%, values even better than 10% are obtained in band centres. However, for point sources the wavelength calibration may be dominated by pointing accuracy.

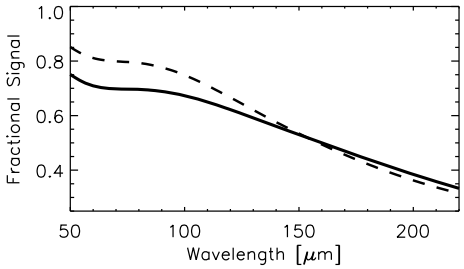

Fig. 9. Point source correction: the fraction of signal seen by the central PACS spectrometer spaxel. Dashed line: theoretical calculation from idealised PSF; solid line: 3rd order polynomial fit to results from rasters on Neptune.

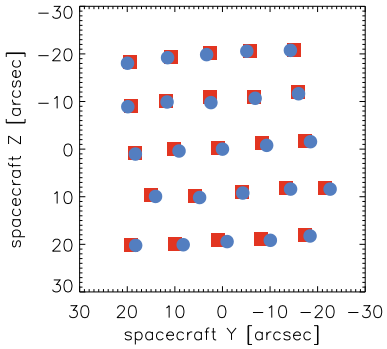

Fig. 10. Spectrometer field of view for blue (circles) and red (squares) spaxels in spacecraft Y and Z coordinates for chopper position zero.

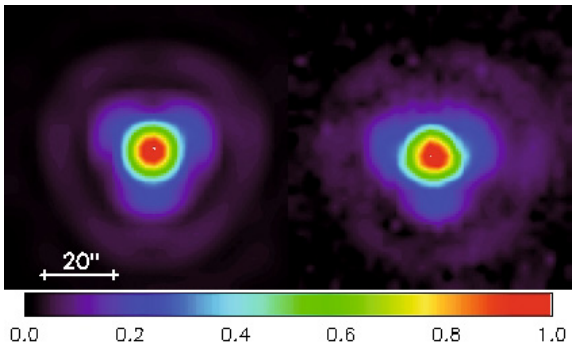

Fig. 11. Calculated spectrometer PSF at 124 μm (*left*) and measurement on Neptune (*right*) done at the same wavelength. Both are normalised to the peak and scaled by square-root, to enhance the faint wing pattern. The calculation includes the predicted telescope wave-front error, which dominates the overall aberrations.

Three 4 × 4 raster observations (3″ step size in instrument coordinates) of the point-like planetary nebula IC 2501 on the atomic fine structure lines [N III] (57 μm), [O III] (88 μm) and [C II] (158 μm) have been compared with predictions from instrument design. Figure 8 shows good agreement between measured spectral line centre positions and the predicted offsets from the relative source position in the slit. Observed wavelength offsets for individual point source observations are therefore expected to fall within the dashed colour lines, given the nominal pointing uncertainty of the spacecraft (Pilbratt et al. 2010).

The pre-launch flux calibration of the spectrometer is based on measurements with the laboratory test cryostat and its test optics. Significant changes to this calibration in flight originate from a major response change of the Ge:Ga photoconductors due to the radiation environment in the L2 orbit, a retuning of the detector bias for optimum sensitivity, and the telescope efficiency. On shorter time scales (one to few hours) the Ge:Ga detectors also show slight drifts in absolute response. Each observation is therefore preceded by a short exposure on the internal calibration sources, which will allow to derive a detector pixel specific relative correction factor. While the laboratory blackbodies could be considered as ideal extended sources covering the entire 47″ × 47″ field of view of the spectrometer, celestial calibration standards are typically point sources. Observations of point-like targets in lower flux regimes can basically sample only the central spatial pixel. A simple diffraction calculation (circular aperture with central obscuration) has been initially adopted to correct point-source fluxes. An improved point source correction has then been derived as a result of extended 100″ × 100″ rasters on Neptune. The results are presented in Fig. 9. After correcting for the increased absolute response (factors 1.3 and 1.1 for blue and red spectrometer respectively), taking the point source correction into account, but without drift correction yet, the absolute flux calibration uncertainty is of order 30%. Improved statistics on results from celestial standards and implementation and use of the results of the internal calibration block in the processing pipeline are in progress.

The spatial calibration of the PACS spectrometer section consists of the detailed characterization of the relative locations on the sky of the 5 × 5 spatial pixels ("spaxels") in the blue and red sections and for all operational chopper positions (±3′, ±1.5′, ±0.5′, 0′). Detailed extended rasters on point sources (HIP21479 and Neptune) have been carried out during PV phase at a few wavelengths and the resulting spaxel geometries are stored as calibration files within the processing software. Figure 10 shows, as an example, the result for chopper position zero in relative spacecraft units with respect to the virtual aperture of the PACS spectrometer, which is defined as the central pixel of the blue field of view. Asymmetrical optical distortions between chopper on and off positions cause unavoidable slight misalignment (≤2″) for individual spaxels between spacecraft nod A and B within the double differential data acquisition scheme.

A further result of extended rasters on Neptune has been the verification of the point spread function of the spectrometer. Remarkable agreement with predictions from telescope and instrument modeling has been found. A measurement for a typical spatial pixel of the PACS spectrometer can be compared in Fig. 11 to a convolution of a calculated PSF (from actual telescope model including known wave-front errors) with a square pixel of 9.4″ × 9.4″.

5. In-orbit performance

The instrument tests executed during *Herschel*'s commissioning phase successfully verified all critical thermal and mechanical aspects. The PACS mechanisms and calibration sources have been tuned to zero gravity conditions and are fully functional. After passing through several weeks of post-launch stabilisation, all thermal interface temperatures reached equilibrium values close to or even better than expectations.

Following the satellite commissioning phase a comprehensive characterisation and calibration programme of the instruments has been executed within the performance verification phase of the *Herschel* mission. As a key pre-requisite to this programme, all PACS detector supply voltages and heater settings had to be optimised for the thermal and space radiation environment as encountered at L2 as well as for the actual far-infrared thermal background emission caused by the temperature

Table 4. Bolometer readout saturation levels (high-gain setting).

Filter	Point source [Jy]	Extended source [GJy/sr]
Blue	220	290
Green	510	350
Red	1125	300

Table 5. Absolute photometric uncertainty and point source sensitivity.

Band	Uncertainty[a]	Point source[b] mode $5\sigma/1$ h	Scan map[b] $[10' \times 15']$ $5\sigma/30$ h	Parallel[b] $[120' \times 120']$ $1\sigma/3$ h
Blue	±10%	4.4 mJy	3.7 mJy	19.8 mJy
Green	±10%	5.1 mJy	5.0 mJy	n.a.
Red	±20%	9.8 mJy	9.5 mJy	116 mJy

Notes. [(a)] Derived from 33, 23 and 51 targets for blue, green and red point source observations respectively.
[(b)] The noise values quoted in the table are instrument limited for the blue and green filter. The value for the red filter already contains confusion noise contributions (see text).

and emissivity of the telescope. The measured glitch rates on the different PACS detectors were compatible with expectations at solar minimum (Ge:Ga photoconductors: 0.08−0.2 hits/s/pixel; Bolometers: ∼1 hit/min/pixel). The observed far-infrared telescope background, mainly determined by M1 and M2 temperatures and the telescope emissivity (see Fischer et al. 2004) was very close to predictions during the first PACS spectrometer measurements.

The measured in-flight performance of the ^{3}He cooler for the bolometers substantially exceeds the required hold time of two days. The cooler hold time, $t_{\rm hold}$, as a function of $t_{\rm on}$, the time during which the bolometers are actually powered-on is: $t_{\rm hold} = 72.97\,{\rm h} - 0.20 \times t_{\rm on}$.

Since the blue PACS photometer offers the highest spatial resolution imaging on-board *Herschel*, it has been used for determining the spacecraft instrument alignment matrix (SIAM) defining the absolute location of all the instruments' virtual apertures and the *Herschel* absolute (APE) and relative (RPE) pointing errors (Pilbratt et al. 2010).

5.1. Photometer

The performance of the photometer expressed as point source sensitivity is listed in Table 5. These numbers are derived from actual science observations. Our best estimate of the confusion-noise free sensitivity for deep integration comes from the scan map, where – at the quoted levels – source confusion is negligible in the blue and green bands, and still minor in the red band. The sensitivity numbers in the other cases – corrected for different integration times – are fully consistent, with the exception of the red band in the parallel mode observation, which is from a shallow galactic plane survey, where source confusion already dominates the noise.

The upper flux limits of the photometer, with the readout electronics in its (default) high-gain setting, are given in Table 4. Above these flux levels the gain will be set to "low", which gives an extra headroom of ∼20%.

SPIRE/PACS parallel mode observations, typically in use on very large fields require additional reduction (signal averaging to 200 ms instead of 100 ms time bins) of blue photometer data.

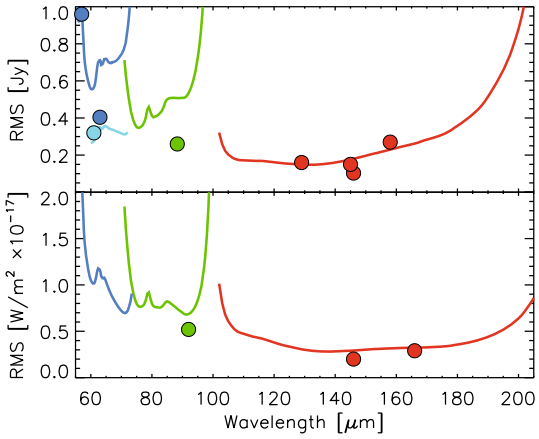

Fig. 12. One sigma continuum sensitivity (*upper plot*) and line sensitivity (*lower plot*) for a number of faint line detections in comparison to the HSPOT predictions for a single Nod and single up-down scan by the grating, with a total execution time of 400...440 s, depending on wavelength. The different colours represent the different spectral PACS bands and grating orders. Nyquist binning (two bins per *FWHM*) has been used to derive the measured line detection sensitivity *in each bin*, while the HSPOT prediction refers to total line flux. Thus, the actual sensitivity values shown here are very conservative.

Together with scan speeds of 60″/s, significant elongations of PSFs in such maps have been measured (Fig. 7), as expected.

The presence of faint (≤1%) optical ghosts and electrical crosstalk was known from instrument level tests and has been reproduced in-flight. Reflections from bright sources by the telescope structure are also known to produce stray-light in the PACS field of view (Pilbratt et al. 2010).

Accurate synchronisation between PACS detector data and spacecraft pointing data is crucial for aligning forward and backward directions of scan map observations and for superposing scan maps obtained in orthogonal directions. There seems to be a systematic delay of 50ms, by which the satellite pointing information is lagging the PACS data. Compensation of this effect is not part of the pipeline and needs to be done "manually".

5.2. Spectrometer

The spectral resolution of the instrument, measured in the laboratory with a methanol far-infrared laser setup (Inguscio et al. 1986), follows closely the predicted values of the PACS observers' manual. Spectral lines in celestial standards (planetary nebulae, HII regions, planets, etc.) are typically doppler broadened to 10−40 km s^{-1}, which has to be taken into account for any in-flight analysis of the spectral resolution. The double differential chop-nod observing strategy leads to slight wavelength shifts of spectral profile centres due to the finite pointing performances. Averaging nod A and nod B data can therefore lead to additional profile broadening causing typical observed *FWHM* values that are up to ∼10% larger.

Characterising the sensitivity of the PACS spectrometer resulted in rms noise values which are compatible with (and mostly better than) pre-launch predictions for all spectroscopic observing modes. Figure 12 provides a comparison of HSPOT sensitivities and several measured values derived from faint line and continuum observations.

The wavelength dependence of the absolute response of each spectrometer pixel is characterised by an individual relative spectral response function. Since this calibration file has

been derived from the extended laboratory black-body measurements, its application to point sources requires additional diffraction corrections. The required correction curve is provided in Fig. 9; however, partly extended sources may consequently show deviating spectral shapes according to their size and morphology. The precision of the relative spectral response is affected by spectral leakage (order overlap due to finite steepness of order sorting filter cut-off edges) from grating order $n + 1$ into grating order n. At wavelengths of 70−73 μm, 98−105 μm and 190−220 μm the next higher grating order wavelengths of 52.5−54.5 μm, 65−70 μm and 95−110 μm do overlap respectively. Continuum shapes and flux densities in these border ranges are therefore less reliable than in band centres.

6. Data analysis and pipeline

The *Herschel* ground segment (*Herschel* common science system – HCSS) has been implemented using Java technology and written in a common effort by the *Herschel* Science Centre and the three instrument teams. One of the HCSS components is the PACS data processing system.

The PACS software was designed for a smooth transition between the different phases of the project, from instrument level tests to routine phase observations. PACS software supported various operation scenarios:

- pipeline processing: pipeline processing is the automatic execution of the standard data processing steps (Wieprecht et al. 2009; Schreiber et al. 2009). Generated products are saved after defined processing levels);
- interactive processing: the PACS standard product generation (SPG/Pipeline) is designed in a modular way. Within the *Herschel* interactive processing environment (HIPE)[4] it is possible to run the pipeline stepwise, change processing parameter, add self-defined processing steps, save and restore the intermediate products, apply different calibrations and inspect the intermediate results. Various GUI tools support the intermediate and final product inspection (Wieprecht et al. 2009; Schreiber et al. 2009).

6.1. Level 0 product generation

Level 0 products are complete sets of data as a starting point for scientific data reduction. Level 0 products may reach a data volume of 750 MB/h (photometer), or 200 MB/h (spectrometer). Depending on the observing mode the data are decompressed and organized in user friendly structures, namely the Frames class for on-board reduced data (holding basically data cubes) and the Ramps class containing typical spectrometer ramp data. Housekeeping (HK) data are stored in tables with converted and raw values (Huygen et al. 2006). Also the full resolution instrument status information (chopper position etc.) is stored as products. Additional data, like the spacecraft pointing, time correlation, and selected spacecraft housekeeping information are provided as auxiliary products. This information is partly merged as status entries into the basic science products. Finally level 0 contain the calibration data needed for data analysis.

[4] HIPE is a joint development by the *Herschel* Science Ground Segment Consortium, consisting of ESA, the NASA *Herschel* Science Center, and the HIFI, PACS and SPIRE consortia. See http://herschel.esac.esa.int/DpHipeContributors.shtml.

6.2. Level 0.5 product generation

Processing until this level is AOT independent. Additional information like processing flags and masks (saturation, damaged pixel, signals affected by chopper and grating transitions) is added, overviews generated, basic unit conversions applied (digital readouts to Volts/s) and for the spectrometer the wavelength calibration (inclusive velocity correction) is done. Also the center of field coordinates are computed for every frame and sky coordinates are assigned for every pixel.

6.3. Level 1 product generation

The automatic data generation of level 1 products is partly AOT dependent. Level 1 processing includes the flux calibration and adds further status information to the product (e.g. chopper angle, masks, etc.). The resulting product contains the instrument effect free, flux calibrated data with associated sky coordinates. These are the biggest products in the processing chain and may reach 3 GB/h for photometry and 2 GB/h in the case of spectroscopy. The spectroscopy level 1 product (PacsCube) contains fully calibrated $n \times 5 \times 5$ cubes per pointing/spectral range. The AOT independent steps in *spectroscopy* are:

- flag glitched signals;
- scale signal to standard capacitance;
- determine response and dark from calibration blocks;
- correct signal non-linearities;
- divide signals by the relative spectral response function;
- divide signals by the response.

Chopped AORs:

- subtract off-source signal from on-source signal;
- combine the nod positions;
- create a PacsCube from PACS spectrometer frames.

Wavelength switching AORs:

- subtract the dark;
- subtract the continuum;
- create a PacsCube from PACS spectrometer frames;
- compute a differential Frames by pairwise differencing;
- fit the differential frames;
- create a synthetic PacsCube based on the fit.

The processing of *photometer* level 1 data is also partly AOT dependent. The resulting product contains a data cube with flux densities and associated sky coordinates stored as a PACS Frames class. Common tasks are:

- process the calibration blocks;
- flag permanently damaged pixels;
- flag saturated signals;
- convert digital readouts to Volts;
- correct crosstalk (currently not activated);
- detect and Correct Glitches;
- derive UTC from on board time;
- convert the digital chopper to angle and angle on sky;
- calculate the centre-of-field coordinates for every frame;
- responsivity calibration.

Chopped point source observations additional tasks:

- flag signals affected by chopper transitions;
- mark dither positions;

- mark raster positions;
- average chopper plateau data;
- calculate central pointing per dither and nod position;
- calculate sky coordinates for every readout;
- compute difference of chopper position readouts;
- average dither positions;
- compute difference of nod positions;
- combine nod data.

6.4. Level 2 Product generation

These data products can be used for scientific analysis. Processing to this level contains actual images and is highly AOT dependent. Specific software may be plugged in. For optimal results many of the processing steps along the route from level 1 to level 2 require human interaction. Drivers are both the choice of the right processing parameters as well as optimising the processing for the scientific goals of the observation. The result is an Image or Cube product.

Spectroscopy processing:

The Spectrometer level 2 data product contains noise filtered, regularly sampled data cubes and a combined cube projected on the WCS. In the case of wavelength switching an additional cube holds the result of the fits.

- generate a wavelength grid for rebinning;
- flag outliers;
- rebin on wavelength grid;
- project the spaxels onto the WCS combining several 5×5 cubes.

Photometry processing:

The PACS software system offers two options for level 2 generation. The simple projection – also used in the automatic pipeline – and MADmap processing, which is available only in the interactive environment as it currently requires significant human interaction.

Simple projection

- HighPass filtering. The purpose is to remove the $1/f$ noise. Several methods are still under investigation. At the moment the task is using a median filter, which subtracts a running median from each readout. The filter box size can be set by the user. This method is optimised for point sources while low spatial frequencies (extended structures) may get suppressed.
- Projection. The task performs a simple coaddition of images, by using a simplified version of the drizzle method (Fruchter & Hook 2002) It can be applied to scan map observations without any particular restrictions.

MADmap

Reconstruction of extended structures requires a different map-making algorithm, which does not remove the low spatial frequencies. PACS adopted the Microwave Anisotropy Dataset mapper for its optimal map making in the presence of $1/f$ noise (Cantalupo & Hook 2010). MADmap produces maximum likelihood maps from time-ordered data streams. The method is based on knowledge of the noise covariance.

In the implementation of MADmap for PACS the noise is represented with an a-priori determined noise model for each bolometer channel. In addition, the correlated (inter-channel) signal is removed prior to map making.

7. Conclusions

With the PACS instrument, we have – for the first time – introduced large, filled focal plane arrays, as well as integral-field spectroscopy with diffraction-limited resolution, in the far infrared. Without any prior demonstration, several major, technological developments have found their first application with PACS in space. The success of this path – documented by the results in this volume – should encourage our community to defend this more "pioneering" approach against trends towards an "industrial" (i.e., minimal-risk) approach, which will not allow us to take advantage of the latest, experimental developments, on which our scientific progress often depends.

Acknowledgements. PACS has been developed by a consortium of institutes led by MPE (Germany) and including UVIE (Austria); KU Leuven, CSL, IMEC (Belgium); CEA, LAM (France); MPIA (Germany); INAF-IFSI/OAA/OAP/OAT, LENS, SISSA (Italy); IAC (Spain). This development has been supported by the funding agencies BMVIT (Austria), ESA-PRODEX (Belgium), CEA/CNES (France), DLR (Germany), ASI/INAF (Italy), and CICYT/MCYT (Spain).
A.P. would like to thank the entire PACS consortium, including industrial partners, for following on this crazy adventure, and T. Passvogel and the Project Team at ESA for tolerating us. F. Marliani's (ESTEC) support in fighting a crucial battle shall never be forgotten.

References

Ade, P. A. R., Pisano, G., Tucker, C., & Weaver, S. 2006, Proc. SPIE, 6275, 62750U
Agnese, P., Buzzi, C., Rey, P., Rodriguez, L., & Tissot, J.-L. 1999, Proc. SPIE, 3698, 284
Agnese, P., Cigna, C., Pornin, J.-L., et al. 2003, Proc. SPIE, 4855, 108
Billot, N., et al. 2007, Proc. SPIE, 6265, 9B
Cantalupo, C. M., Borrill, J. D., Jaffe, A. H., Kisner, T. S., & Stompor, R. 2010, ApJS, 187, 212
Dehaes, S., Bauwens, E., Decin, L., et al. 2010, A&A, submitted
Duband, L., Clerc, L., Ercolani, E., Guillemet, L., & Vallcorba, R. 2008, Cryogenics, 48, 95
Fischer, J., Klaassen, T., Hovenier, N., et al. 2004, App. Opt., 43, 3765
Fletcher, L. N., Drossart, P., Burgdorf, M., et al. 2010, A&A, 514, A17
Fruchter, A. S., & Hook, R. N. 2002, PASP, 114, 144
Huygen, R., Vandenbussche, B., & Wieprecht, E. 2006, ASP Conf. Ser., 351, 220
Inguscio, M., Moruzzi, G., Evenson, K., & Jennings, D. 1986, J. Appl. Phys., 60, 161
Katterloher, R., Barl, L., Poglitsch, A., Royer, P., & Stegmaier, J. 2006, Proc. SPIE, 6275, 627515
Kraft, S., Frenzl, O., Charlier, O., et al. 2000, Proc. SPIE, 4013, 233
Kraft, S., Merken, P., Creten, Y., et al. 2001, Proc. SPIE, 4540, 374
Krause, O., Lemke, R., Hofferbert, R., et al. 2006, Proc. SPIE, 6273, 627325
Looney, L. W., Raab, W., Poglitsch, A., & Geis, N. 2003, ApJ, 597, 628
Merken, P., Creten, Y., Putzeys, J., Souverijns, T., & Van Hoof, C. 2004, Proc. SPIE, 5498, 622
Müller, T. G., & Lagerros, J. S. V. 1998, A&A, 338, 340
Müller, T. G., & Lagerros, J. S. V. 2002, A&A, 381, 324
Ottensamer, R., & Kerschbaum, F. 2008, Proc. SPIE, 7019, 70191B
PACS observers' manual 2010, http://herschel.esac.esa.int/Docs/PACS/pdf/pacs_om.pdf
Pilbratt, G. L., et al. 2010, A&A, 518, L1
Poglitsch, A., Katterloher, R. O., Hoenle, R., et al. 2003, Proc. SPIE, 4855, 115
Poglitsch, A., et al. 2006, Proc. SPIE, 6265, 62650B
Poglitsch, A., et al. 2008, Proc. SPIE, 7015, 701005
Poglitsch, A., & Altieri, B. 2009, EAS Publ. Ser., 34, 43
Renotte, E., Gillis, J.-M., Jamar, C. A., et al. 1999, Proc. SPIE, 3759, 189
Schreiber, J., Wieprecht, E., de Jong, J., et al. 2009, ASP Conf. Ser., 411, 478
Schulz, B., Huth, S., Laureijs, R. J., et al. 2002, A&A, 381, 1110
Shirahata, M., Matsuura, S., Hasegawa, S., et al. 2009, PASJ, 61, 737
Simoens, F., Agnese, P., Béguin, A., et al. 2004, Proc. SPIE, 5498, 177
Stegmaier, J., Birkmann, S., Grözinger, U., Krause, O., & Lemke, D. 2008, Proc. SPIE, 7010, 701009
Wieprecht, E., Schreiber, J., de Jong, J., et al. 2009, ASP Conf. Ser., 411, 531